Magnetic and neutron diffraction study of $La_{2/3}Ba_{1/3}MnO_3$ perovskite manganite

A. B. Beznosov, V. A. Desnenko, and E. L. Fertman*
B. Verkin Institute for Low Temperature Physics and Engineering, National Academy of Sciences of Ukraine, 47 Lenin Avenue, 61103 Kharkov, Ukraine

C. Ritter
Institut Laue-Langevin, Boîte Postale 156, 38042 Grenoble Cedex 9, France

D. D. Khalyavin
Institute of Physics of Solids and Semiconductors, National Academy of Sciences, 17 P. Brovka Street, 220072 Minsk, Belarus
(Received 16 August 2002; revised manuscript received 31 March 2003; published 22 August 2003)

The evolution of the magnetic and structural properties of $La_{2/3}Ba_{1/3}MnO_3$ perovskite manganite was studied as a function of temperature by means of dc magnetic measurements at zero pressure as well as under uniaxial pressure of 0.1 kbar and neutron-diffraction between 5–370 K. It was revealed that below the Curie point $T_C = 314$ K in addition to the main crystallographic phase possessing a rhombohedral structure $R\bar{3}c$ some amount of the orthorhombic *Imma* phase appears in the system. The system undergoes three magnetic phase transitions in low magnetic fields (of the second order at 300 and 250 K and of the first order at 177.5 K) and passes via a sharp but not complete structural transition $R\bar{3}c \leftrightarrow Imma$ in the vicinity of $T_e = 200$ K. The reduced change of magnetic susceptibility $\Delta\chi/\chi$ under uniaxial pressure displays a sharp minimum at temperature T_e. Below the Curie temperature from 300 to 250 K the magnetic susceptibility χ is independent of the temperature, which is considered as an indication of a probable formation below $T_h = 300$ K of a long period magnetic structure (probably a sort of low-angle helix).

DOI: 10.1103/PhysRevB.68.054109 PACS number(s): 75.30.−m, 75.80.+q, 75.47.De

I. INTRODUCTION

The mixed-valence perovskite manganites $A_{1-x}A'_xMnO_3$ with A = La, A′ = Ca, Sr, Ba, have recently attracted considerable attention because of a huge negative magnetoresistance (a ''colossal magnetoresistance''—CMR) near the Curie temperature. A number of works has recently been devoted to studying the interplay between structure, magnetism, and transport in manganese perovskites.[1–6] This system displays a rich variety of magnetotransport and structural properties as a function of temperature, applied magnetic field, doping, applied pressure, mean *A*-site ionic radius r_A.

The main crystal and spin structures of manganites $A_{1-x}A'_xMnO_3$ for different x were found by Wollan and Koehler by neutron-diffraction study in 1955.[7] They were in a good agreement with Goodenough[8] calculations and became generally accepted. It was shown that increasing the doping brings about a significant change of the magnetic order, of the type AFM-FM-AFM (where FM means, ferromagnetic and AFM means antiferromagnetic). For certain values of the electronic doping $0.2 < x < 0.5$ these compounds are metallic and ferromagnetic at low temperatures, while their conductivity displays semiconducting behavior at high temperatures. The metal-insulator transition between these two states is strongly coupled with the magnetic ordering transition: the metal-insulator transition temperature coincides with the Curie temperature T_C. These compounds display CMR, and the largest value of the effect is observed around the $x \approx 0.34$ interval of concentrations of the divalent metal. The appearance of metallic ferromagnetism on doping has been explained by the mechanism of the double-exchange interaction.[9,10] Recent theoretical work indicated the need to consider a strong electron-lattice coupling, due to dynamic Jahn-Teller distortions of the lattice, in order to account the colossal magnetoresistance effect that these materials exhibit.[11]

The short-range magnetic correlations above T_C lead to the formation of magnetic polarons,[5] which are precursors of the developing magnetic inhomogeneity (phase segregation).[12]

Below the Curie temperature a magnetic inhomogeneity is characteristic for mixed valence manganites; it was clearly shown by several techniques such as neutron scattering,[13,14] tunneling microscopy,[15] nuclear magnetic resonance,[16] ferromagnetic resonance (FMR),[17] x-ray-diffraction studies.[18] Insulating and metallic domains of 10–50 nm coexist and percolate as a function of temperature and applied magnetic field.

A number of studies has concentrated recently on the effect of the mean *A*-site ionic radius on the magnetic and magnetotransport properties.[1,2,6,19] When the doping of the *A* site with bivalent ions is kept constant, the main effect of the *A*-site substitution is to change the structural parameters, such as Mn-O-Mn bond angles and Mn-O bond lengths. The ionic radii of the constituent ions are known to determine the kind and degree of distortion of the simple cubic perovskite structure.[20] The T_C of perovskite manganites $A_{1-x}A'_xMnO_3$ can be continuously varied by various substitutions. But the Curie temperature is a nonmonotonic function of r_A, reaching a maximum for the composition $La_{2/3}Sr_{1/3}MnO_3$ ($r_A \approx 1.24$ Å). The Ba-doped manganites possess the largest value $r_A \approx 1.292$ Å (Ref. 6) among the $A_{1-x}A'_xMnO_3$ manganites which leads to an intrinsically strained structure with crystal lattice parameters close to that of the ideal simple

TABLE I. Refined structural parameters from neutron powder-diffraction data for the phase of the $La_{2/3}Ba_{1/3}MnO_3$ compound having $R\bar{3}c$ space-group symmetry at 5–370 K temperature range. The columns "Err" present statistical errors, and the last column presents the crystal phase volume per formula unit ($V_{f.u.}=(\sqrt{3}/12)a^2c$).

T (K)	a (Å)	Err a ($\times 10^{-4}$ Å)	C (Å)	Err c ($\times 10^{-3}$ Å)	$V_{f.u.}$ (Å^3)
5	5.5203	3.4	13.483	1.46	59.303
100	5.5215	3.2	13.486	1.25	59.342
140	5.5237	3.5	13.487	1.32	59.394
170	5.5249	2.7	13.491	1.08	59.437
190	5.5269	2.1	13.493	0.90	59.489
210	5.5288	1.2	13.497	0.54	59.548
230	5.5297	0.8	13.500	0.36	59.580
250	5.5308	0.7	13.503	0.28	59.617
300	5.5339	0.7	13.513	0.20	59.728
370	5.5387	0.8	13.531	0.26	59.912

cubic perovskite with the average Mn-O-Mn bond angle increased towards values closer to 180°.[19] It was accepted that the $La_{2/3}Ba_{1/3}MnO_3$ manganite crystallizes in rhombohedral ($R\bar{3}c$) crystal lattice at room temperature and in orthorhombic lattice of *Imma* space-group symmetry at 1.6 K.[6] The compound seemed to be possessing at the first sight a simple magnetic phase diagram (at normal pressure $La_{2/3}Ba_{1/3}MnO_3$ was considered to be a paramagnetic insulator above T_C and a ferromagnetic metal below this temperature) and had a magnetoresistance peak in the vicinity of T_C.[21,22]

It is well known, however,[23] that manganese oxides are favorable to a long-period magnetic structure ($L_h \gg c, L_h$ and c are the magnetic superstructure and crystal structure periods, respectively) due to combined exchange-relativistic interactions. Direct observation of a long-period magnetic superstructure by conventional techniques (for example, by neutron diffraction with an acceptable resolution) require perfect crystals of a size $L \gg L_h$. However, as it was mentioned above, real CMR manganites possess magnetic clusters of size $L \approx 10$–50 nm (i.e., approximately 10–50 periods along the long axis of the crystal lattice, that is about, or even less, than L_h, see Tables I and II, and Appendix B), so the requirement $L \gg L_h$ cannot be provided in such systems. At these circumstances, one of the ways to detect a long-period magnetic superstructure is to use characteristic features of their magnetic behavior. For an antiferromagnetic helix such a feature is connected with an independence of the magnetic susceptibility on temperature and magnetic field.[24,25] Certain indication of the magnetic behavior of this type was recently found when studying magnetization of $La_{2/3}Ba_{1/3}MnO_3$.[26] Hence, goal of this paper is to investigate characteristic features of magnetic behavior of $La_{2/3}Ba_{1/3}MnO_3$ by both magnetic and neutron-diffraction techniques from the point of view of possibility of realization of a long-period magnetic structure in this oxide.

In general, mixed valence oxides are very sensitive to applied pressure. The pressure dependence of magnetic properties of various mixed-valence manganites was studied earlier, but the attention was mainly paid to the hydrostatic pressure effects near T_C.[2,6] We have used the effect of low

TABLE II. Refined structural parameters from neutron powder-diffraction data for the phase of $La_{2/3}Ba_{1/3}MnO_3$ compound having *Imma* space-group symmetry at 5–300 K temperature range. The columns "Err" present statistical errors, and the last column presents the crystal phase volume per formula unit ($V_{f.u.}=abc/4$).

T (K)	a (Å)	Err a ($\times 10^{-4}$ Å)	b (Å)	Err b ($\times 10^{-4}$ Å)	c (Å)	Err c 10^{-4} Å	$V_{f.u.}$ (Å^3)
5	5.5102	0.9	7.7893	1.6	5.5323	0.7	59.362
100	5.5118	0.9	7.7919	1.7	5.5326	0.8	59.403
140	5.5133	0.9	7.7948	1.7	5.5330	0.8	59.445
170	5.5147	1.0	7.7974	2.0	5.5335	0.9	59.486
190	5.5157	1.1	7.7992	2.2	5.5338	1.1	59.513
210	5.5171	1.7	7.8012	3.2	5.5338	2.0	59.544
230	5.5184	2.7	7.8036	4.7	5.5336	2.9	59.574
250	5.5201	3.0	7.8056	5.1	5.5328	3.1	59.599
300	5.5267	37.4	7.8102	7.4	5.5302	36.0	59.677

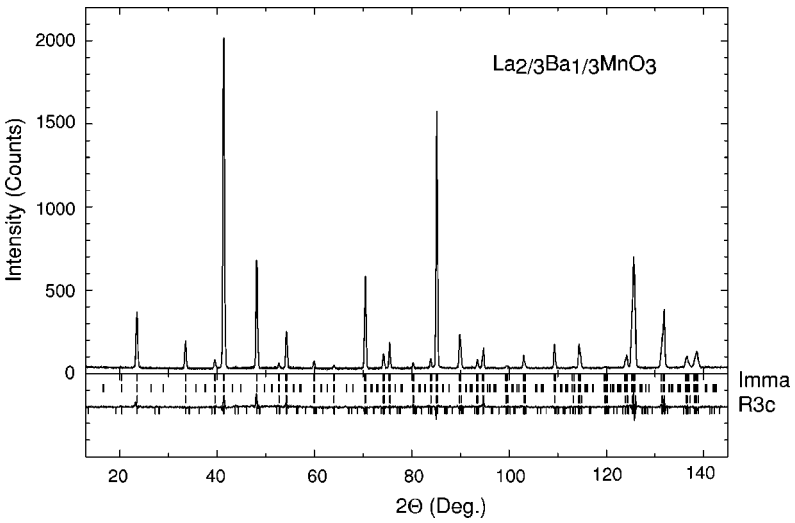

FIG. 1. Two-phase Rietveld refinement of the neutron powder-diffraction data at $\lambda = 1.594$ Å of $La_{2/3}Ba_{1/3}MnO_3$ at 210 K. The tick marks below the profiles indicate the positions of the *Imma* and $R\bar{3}c$ allowed reflections. The difference plot (observed minus calculated profiles) is plotted at the bottom.

uniaxial pressure on magnetic properties to study the stability of the electron and magnetic systems of $La_{2/3}Ba_{1/3}MnO_3$ at low temperatures.

In this work, we present a detailed study of the magnetic and structural properties of $La_{2/3}Ba_{1/3}MnO_3$ perovskite in the 5–370 K temperature region.

II. EXPERIMENT

The studied bulk polycrystalline samples $La_{2/3}Ba_{1/3}MnO_3$ were prepared by standard solid-state reaction from stoichiometric amounts of powders La_2O_3, $BaCo_3$, and Mn_2O_3. After prefiring at 900 °C, the mixture was pressed in the form of tablet and sintered at 1470 °C for 10 h. The samples were cooled slowly with a furnace at a rate of 80 °C h^{-1}. X-ray diffraction indicated a single-phase material.

The measurements of *dc* magnetization *M* were carried out on the toroidal sample (demagnetization factor $N=0$) by means of pulse-induction technique in a low magnetic field $0.01 \leqslant H \leqslant 4.2$ Oe, the studied temperature range was 5–350 K.

The effect of uniaxial pressure *P* of 0.1 kbar on *dc* magnetic susceptibility was measured in the temperature range $5 \leqslant T \leqslant 270$ K in the external magnetic field $H_0 = 20$ Oe by means of superconducting quantum interference device magnetometer. The corresponding installation and experimental technique are similar to those described in Ref. 27. The sample size was $2.55 \times 2.31 \times 1.1$ mm^3, and the demagnetization factor, respectively, was $N \approx 5.4$ in the short side direction, along which the external magnetic field as well as a uniaxial pressure were applied.

The reduced change $\Delta\chi/\chi$ of the magnetic susceptibility $\chi = M/H$ of $La_{2/3}Ba_{1/3}MnO_3$ under the uniaxial pressure was found as following:

$$\frac{\Delta\chi(H,T)}{\chi(H,T)} = \frac{\chi(H,T)}{\chi_N(H_0(H,T))} \frac{\Delta\chi_N(H_0(H,T))}{\chi_N(H_0(H,T))}. \qquad (1)$$

Here, χ_N is the experimentally measured magnetic susceptibility of the sample with the demagnetization factor *N* and *H* is an effective inner magnetic field in the sample. Values $\chi(H,T)$ in Eq. (1) were obtained using the measurements with toroidal sample.

Temperature-dependent neutron powder-diffraction data ($5 \leqslant T \leqslant 370$ K) were obtained using the D1B and D2B diffractometers of the Institute Laue-Langevin equipped with an ILL cryofurnace. Data were obtained at wavelengths $\lambda = 2.5$ Å and $\lambda = 1.594$ Å, respectively, and the last were refined using the program FULLPROF.[28] As an example, the Rietveld plot for $La_{2/3}Ba_{1/3}MnO_3$ at 210 K is shown in Fig. 1. The refinement of the temperature dependent D1B data was complicated because the resolution was not sufficient to see two temperature-driven crystal phases and to refine their nuclear coordinates.

III. STRUCTURAL CHARACTERIZATION

The $La_{2/3}Ba_{1/3}MnO_3$ lattice constants and crystal volumes per Mn atom at different temperatures are reported in Table I and Table II.

At high temperature (370 K), the studied manganite possesses the rhombohedral unit cell (space group $R\bar{3}c$), but "slowly" the phase transition $R\bar{3}c \rightarrow Imma$ is starting near T_C and at 300 K about 12% of orthorhombic phase (space group *Imma*) was registered simultaneously with the rhombohedral phase. With further cooling the amount of the *Imma* crystal phase grows nonuniformly and the amount of the $R\bar{3}c$ phase decreases correspondingly (Fig. 2). Approximately, equal phase fractions of the $R\bar{3}c$ and *Imma* are found at about 200 K. Even at low temperatures there are about 12% of nontransformed phase $R\bar{3}c$ (Fig. 2).

The volumes of formula units of $La_{2/3}Ba_{1/3}MnO_3$ in the structure phases of the $R\bar{3}c$ and *Imma* space-group symmetry in the 5–370 K temperature range are presented in Fig. 3. As one can see, the $R\bar{3}c$ phase volume changes with temperature less uniformly than that of the *Imma* phase. This reflects evidently the presence of more strong temperature changes in the interatomic interactions in this phase. Figure 4 demonstrates the individual sensitivity of the *a* and *c* lattice parameters to the above-mentioned interactions.

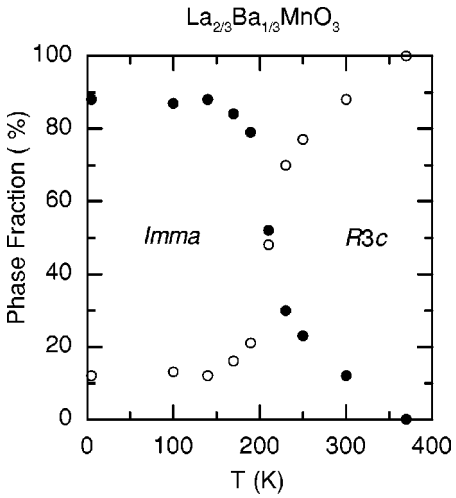

FIG. 2. The phase fraction of *Imma* and $R\bar{3}c$ crystal phases for $La_{2/3}Ba_{1/3}MnO_3$ at 5-370 K.

The temperature behavior of *Imma* lattice parameters is shown in Fig. 5. They possess less expressed temperature anomalies than those of the $R\bar{3}c$ phase and tend to become cubic as the temperature increases.

IV. MAGNETIC PROPERTIES

A. Magnetic susceptibility

The temperature dependence of dc magnetic susceptibility $\chi = M/H$ of $La_{2/3}Ba_{1/3}MnO_3$ when cooling and heating in magnetic field $H = 2.2$ Oe is presented in Fig. 6. The temperature of magnetic ordering was found to be $T_C = 314$ K by extrapolation to $\chi = 0$ of the linear part of the dependence $\chi^2 = \text{const}(T - T_C)$ above 300 K.

It was revealed that below T_C low-field magnetic susceptibility of $La_{2/3}Ba_{1/3}MnO_3$ compound is rather unusual (Fig. 6). At 300 K $\chi(T)$ has a small maximum and between 300 and 250 K the $\chi(T)$ dependence represents an ideal plateau, which is not characteristic for a simple ferromagnetic structure. Furthermore, below 300 K the studied manganite undergoes two magnetic phase transitions: at $T_{II} = 250$ K (of the second order) and at $T_I = 177.5$ K (of the first order). At $T_{II} = 250$ K the temperature derivative of low-field magnetic susceptibility $\partial\chi/\partial T$ has a break; the temperature $T_I = 177.5$ K was determined as an average point of the 15-deg hysteresis loop, at both sides of which the susceptibility χ has a break.

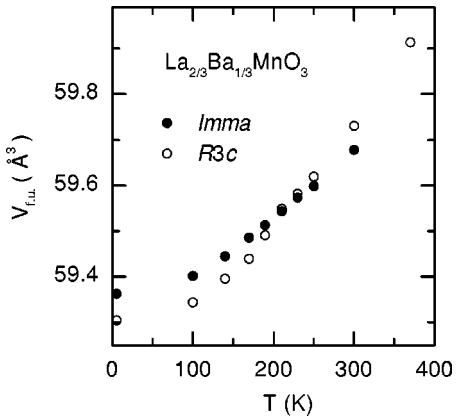

FIG. 3. The volumes of formula units of $La_{2/3}Ba_{1/3}MnO_3$ in the structure phases of the $R\bar{3}c$ and *Imma* space-group symmetry in the 5-370 K temperature range.

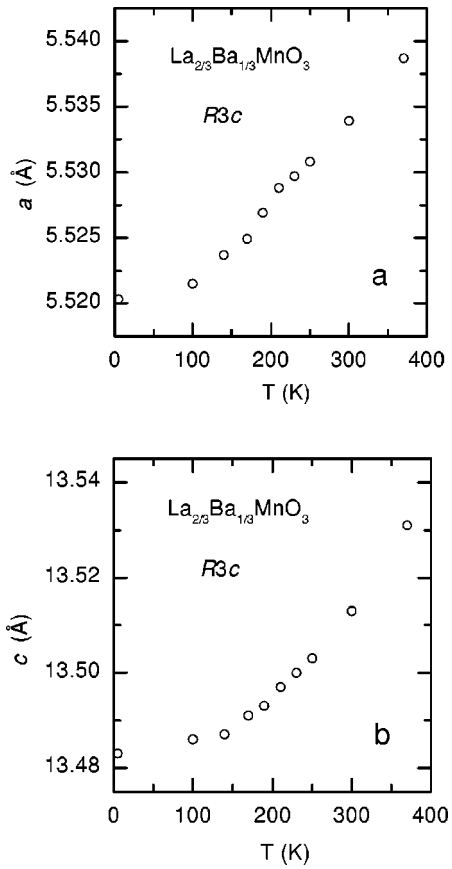

FIG. 4. Temperature dependences of the $R\bar{3}c$ lattice constants.

The revealed magnetic phase transitions take place at low magnetic fields only and are not seen in saturation fields (3–4 kOe,[29]) where the $\chi(T)$ dependence follows a Brillouin-like function.

The field dependences $\chi(H)$ for the nitrogen and room temperatures are presented in Fig. 7. The dashed lines represent an empirical formula for the susceptibility (see Appendix A).

The last gives a magnitude of the susceptibility in an arbitrary point of the field interval considered, that allows to exclude the effects of demagnetization fields when processing the experimental data and to calculate an effect of uniaxial pressure in a substance using Eq. (1).

As can be seen in Fig. 7, the χ value does not change substantially when increasing the magnetic field at $H > 1$ Oe (the corresponding magnetization-field curve $M(H)$ has a zero curvature in this region). Therefore, the dependence $\chi(H)$ at $H > 1$ Oe describes neither process of the ferromagnetic domains boundaries movement (for which a positive curvature $\partial^2\chi/\partial H^2$ is characteristic) nor the process of the ferromagnetic saturation (with a positive curvature

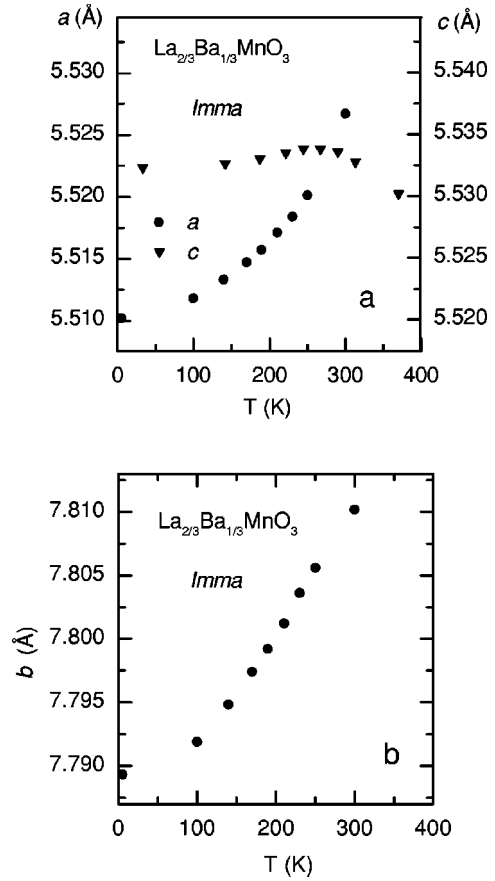

FIG. 5. Temperature dependences of the *Imma* lattice constants.

$\partial^2\chi/\partial H^2$ also). Thus, the $\chi(H)$ curve found has an intradomain character, i.e., reflects the behavior of a single-domain magnetization. But in such a case, magnetic susceptibility of a simple ferromagnetic structure has to be temperature dependent only in the region studied because of the temperature dependence of the magnetization. For a simple ferromagnetic structure, the temperature dependence of the reduced magnetization in the molecular-field model can be expressed as

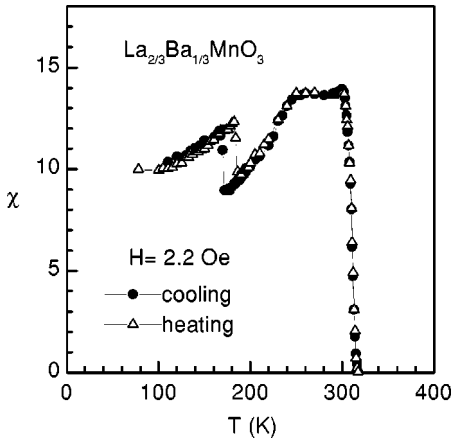

FIG. 6. The dc magnetic susceptibility $\chi=M/H$ of $La_{2/3}Ba_{1/3}MnO_3$ versus temperature when cooling and heating in magnetic field $H=2.2$ Oe.

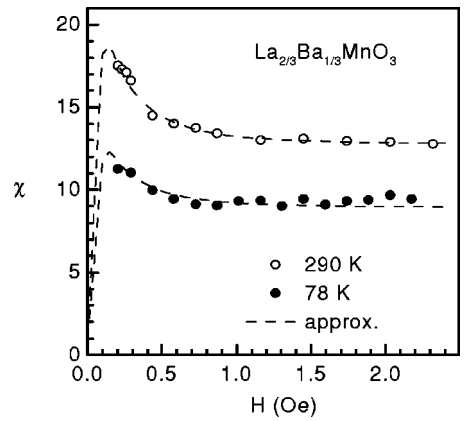

FIG. 7. The dc magnetic susceptibility $\chi=M/H$ of $La_{2/3}Ba_{1/3}MnO_3$ versus magnetic field at the nitrogen and room temperatures.

$$\frac{M}{M_0}=B_S\left(\frac{3S}{S+1}\frac{M}{M_0}\frac{T_C}{T}\right), \tag{2}$$

where B_S is the Brillouin function, S is the spin of the system, and M_0 is the spontaneous magnetization at $T=0$. The low-field magnetic susceptibility $\chi=M/H$ in some related oxides (for example, in the $La_{2/3}Ca_{1/3}MnO_3$ manganite with the polydomain polycrystalline microstructure,[30] similar to that in the present work) follows to Eq. (2) type dependence, and the susceptibility of $La_{2/3}Ba_{1/3}MnO_3$ in the fields exceeding 3–4 kOe does so as well.[29] But the low-field susceptibility of $La_{2/3}Ba_{1/3}MnO_3$ cannot be evidently described by the dependence like Eq. (2).

The experimental value of the magnetic susceptibility of the studied manganite is $\chi\approx 10$. Such a value usually is characteristic of soft ferromagnets, but it may be obtained as well in the framework of a long-period helix model (see Appendix B). Moreover, in contrast to a simple ferromagnetic case, this model gives χ independent of temperature and magnetic field.[24,25,31] Since the data obtained (the magnetic susceptibility independent of field and temperature in the certain intervals of their values) cannot be attributed to a simple ferromagnetic structure and are characteristic of a magnetic helix, one can suppose that the magnetic structure of $La_{2/3}Ba_{1/3}MnO_3$ is helical. If such a helix really exists, its period may be estimated as $L_h\approx 240$ Å using the experimental values of χ and T_C, and also value of the spin and the number of the nearest neighbors of the Mn ion (see Appendix B).

B. Neutron diffraction

General picture of Bragg peaks caused by the nuclear and magnetic scattering of the neutrons with the wavelength $\lambda=2.5$ Å in $La_{2/3}Ba_{1/3}MnO_3$ is presented in Fig. 8 in the coordinates intensity–diffraction angle–temperature. The temperature dependence of the integrated intensity $I(T)$ of magnetic Bragg peak of $La_{2/3}Ba_{1/3}MnO_3$ is presented in Fig. 9. Neutron-diffraction data clearly show the onset of magnetic

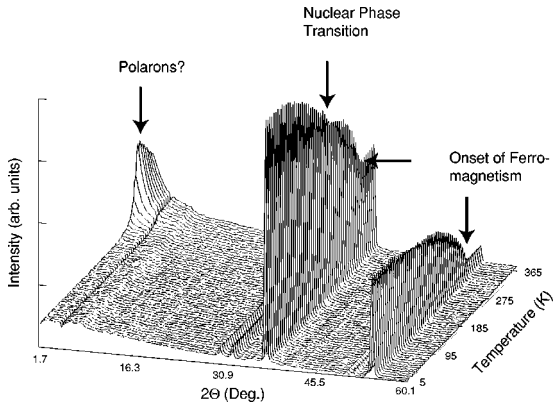

FIG. 8. General picture of Bragg peaks, caused by the nuclear and magnetic scattering in $La_{2/3}Ba_{1/3}MnO_3$ at the wavelength $\lambda = 2.5$ Å, in the coordinates intensity—diffraction angle–temperature.

order at 314 K (Figs. 8 and 9). For a powder sample such a sharp transition indicates the high quality and uniformity of the sample.

At low angles (Fig. 8) a magnetic peak was observed, which disappeared at the Curie temperature. It should be connected to magnetic polarons:[5] they disappear as the system gets long-range magnetic ordered.

As can be seen in Fig. 9, except the Curie temperature there is only one well visible singular point at 200 K (it corresponds to the ''electronic transition'' temperature T_e, being discussed in Sec. V). The phase transitions at 250 K and 175 K are not reflected in the intensity of this diffraction peak. The experimental magnetic Bragg peak intensity goes higher than the curve described by the Brillouin function

$$\frac{\Delta I}{\Delta I_0} = \sigma^2 = B_S^2\left(\frac{3S}{S+1}\frac{T_C}{T}\sigma\right), \tag{3}$$

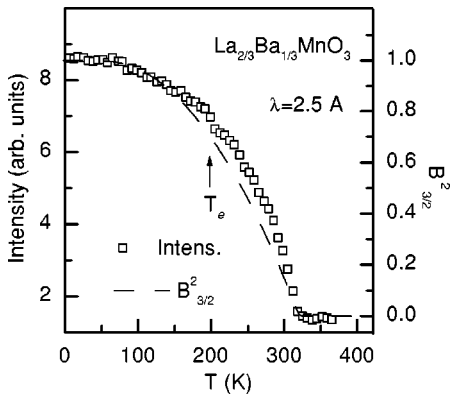

FIG. 9. Temperature dependence of the integrated intensity of magnetic Bragg peak (□) in $La_{2/3}Ba_{1/3}MnO_3$, obtained from the neutron-diffraction data at the wavelength $\lambda = 2.5$ Å. The dashed line represents square of the Brillouin function for spin 3/2 [Eq. (3)](---). The arrow points out the ''electronic transition'' temperature (see Sec. V). The Bragg peak seen is a combination of the 200/121 peaks of *Imma* and of the 110/104 peaks of $R\bar{3}c$.

where $\Delta I = I(T) - I(370\ \mathrm{K})$, $\Delta I_0 = I(5\ \mathrm{K}) - I(370\ \mathrm{K})$, $S = 3/2$ is the spin of the Mn^{4+} ion, and $T_C = 314$ K. Such a behavior is expectable for double-exchange systems.[32]

The experiment carried out had no sufficient conditions to observe the supposed magnetic helix. Though its parameters look enough realistic, they are not appropriate for the present experimental study since the period of the structure and the sizes of metallic domains in such systems (10–50 nm) are of the same order (see Appendix C). The peaks, corresponding to a helix with period $L_h = 240$ Å should occur very close to the direct beam and very close to the main Bragg reflections. The difference to a normal ferromagnetic structure should not be visible. A small-angle neutron-diffraction study could detect the main satellite close to the 000 position, however, the small domain size would prohibit a strong coherent signal from the possible helix and lead at the same time to nuclear small-angle scattering.

Thus, a simple model with collinear Mn moments, which should be considered as an ''equivalent'' ferromagnetic in case if the real magnetic structure represents a long-period superstructure (see Appendix C), was used to describe the magnetic scattering. ''Effective'' magnetic moments of the Mn ions were refined from the data at $\lambda = 1.594$ Å (see Sec. II). In any case, they correspond to the projection of the spin of Mn ion onto a local quantization axis, which is equivalent to a Z axis of the laboratory frame of reference if the magnetic structure is simple ferromagnetic (see Appendix C).

At 5 K the ordered magnetic moment, based on the nuclear and magnetic intensities of Bragg peaks, was $\mu = 3.40 \pm 0.03 \mu_B$, as was expected for the studied Mn^{3+}/Mn^{4+} system. Temperature dependence of the reduced effective magnetic moment μ/μ_0 per Mn atom is presented in the Fig. 10(a) together with curves described by a modified Brillouin curve,[30]

$$\sigma = B_S\left(\frac{3S}{S+1}\frac{T_C(1+e\sigma^2)}{T}\sigma\right), \tag{4}$$

for spin $S = 3/2$, $T_C = 314$ K, and the fitting parameters $e = 0$, 0.2, and 0.4. Figure 10(b) presents the temperature dependences of the deviations Δ_μ of μ/μ_0 from the conventional ($e = 0$) and moderately modified ($e = 0.2$) Brillouin functions.

As can be seen in Fig. 10(a), the general run of the effective magnetic moment with temperature radically differs from that one represented in Fig. 6. The last dependence is supposed to be attributed to the single-domain magnetization of a low-field noncollinear magnetic superstructure. The observed difference between the dependences in Figs. 6 and 10(a) implies that the real low-field magnetic structure in $La_{2/3}Ba_{1/3}MnO_3$ is not collinear ferromagnetic. In the saturating fields exceeding 3–4 kOe, destroying any low-field complex magnetic structure, the magnetization-temperature dependence[29] looks similar to the dependence in Fig. 10(a).

Another important feature of the dependence in Fig. 10(a) is a very sharp growth of μ just below the Curie point: the experimental data are well fitted by the strongly modified Brillouin curve described by Eq. (4) with $e = 0.4$. As can be seen in Figs. 10(a) and 10(b), at 300 K the μ/μ_0 value is

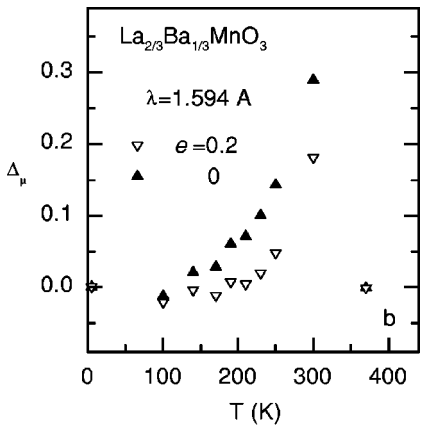

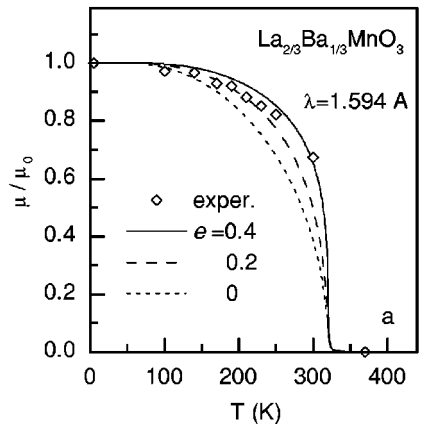

FIG. 10. (a) Temperature dependences of the reduced "effective" magnetic moment μ/μ_0 ($\diamond$) per Mn atom in $La_{2/3}Ba_{1/3}MnO_3$, obtained from the neutron-diffraction data at the wavelength $\lambda = 1.594$ Å. Solid, dashed, and dotted lines represent a strongly ($e=0.4$) and a moderately ($e=0.2$) modified Brillouin functions $B_S(e)$ [30] for spin $S=3/2$, and the conventional Brillouin function ($e=0$), respectively. (b) Temperature dependences of the deviations Δ_μ of μ/μ_0 from the conventional ($\blacktriangle$) and moderately modified (∇) Brillouin functions.

37% higher than M/M_0 in $La_{2/3}Ca_{1/3}MnO_3$ system,[30] which is rather well described by Eq. (4) with $e=0.2$, and 75% higher than the corresponding value given by the conventional Brillouin function [Eq. (4) with $e=0$]. A temperature dependent molecular-field parameter in the double-exchange systems, giving similar effects, was considered earlier in the paper.[32]

C. Uniaxial pressure effect

The pressure dependence of magnetic properties of various mixed-valence doped manganites was studied earlier, but the attention was mainly paid to the hydrostatic pressure effects near T_C. The ferromagnetic state is usually stabilized by the hydrostatic pressure application, with $dT_C/dP \approx 10-30$ K/GPa.[2] At the same time, the effect on T_C of hydrostatic pressure and chemical pressure (achieved by substitution smaller *A*-site cations) are opposite. It can be explained since pressure increases the Mn-Mn overlap integral and bandwidth, thereby enhancingT_C; smaller *A*-site cations tend to reduce the Mn-O-Mn bond angles, hence diminishing the transfer integral.[2]

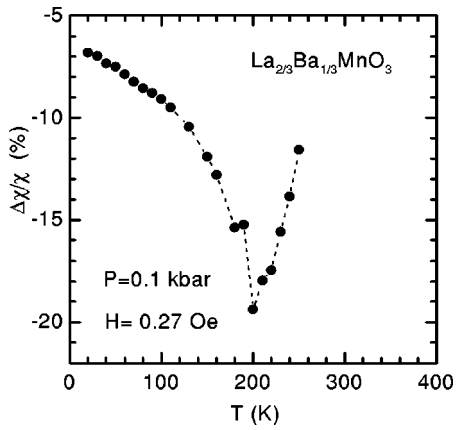

FIG. 11. Reduced change $\Delta\chi/\chi$ of the dc magnetic susceptibility $\chi = M/H$ of $La_{2/3}Ba_{1/3}MnO_3$ versus temperature when heating under the uniaxial pressure $P=0.1$ kbar at the effective inner magnetic field 0.27 Oe.

In the present study, we use low uniaxial pressure (0.1 kbar) to reveal temperature regions of the electron structure instability and phase transitions. A magnitude of the effect for an unbounded substance was calculated using the magnitude of the effect in the studied sample and Eqs. (1) and (A1). It was found that the reduced change of the magnetic susceptibility under the uniaxial pressure $\Delta\chi/\chi$ of $La_{2/3}Ba_{1/3}MnO_3$ is negative all over the studied temperature range (Fig. 11) and appeared to be very sensitive to the changes in magnetic and lattice state of the compound. The temperature dependence of the $\Delta\chi/\chi$ has a sharp minimum at $T=200$ K. At about 185 K, the $\Delta\chi/\chi(T)$ curve demonstrates a change of a slope (Fig. 11), it is probably connected with the first-order magnetic phase transition at $T_1=185$ K when heating (Fig. 6).

V. ANALYSIS OF THE PHASE TRANSFORMATIONS

Crystal volume as a function of temperature can be represented as a sum of two contributions

$$V_{f.u.}(T) = V_{DG}(T) + V_{mag}(T),$$

where $V_{DG}(T)$ is Debye-Grüneisen term, caused by the unharmonicity of atomic thermal oscillations for an ideal crystal, and $V_{mag}(T)$ is a contribution from magnetic phase transformations (they are the main ones in the temperature region being considered). Supposing, that the low-temperature part of $V_{f.u.}(T)$ dependence of the *Imma* phase is less deformed by magnetic phase transitions, one can choose $V_{f.u.}(5\ \mathrm{K})$ and $V_{f.u.}(100\ \mathrm{K})$ for this phase as parameters determining two of three constants in the expression for $V_{DG}(T)$,

$$V_{DG} = V_0 + A\frac{T}{\theta_D} D\left(\frac{\theta_D}{T}\right). \quad (5)$$

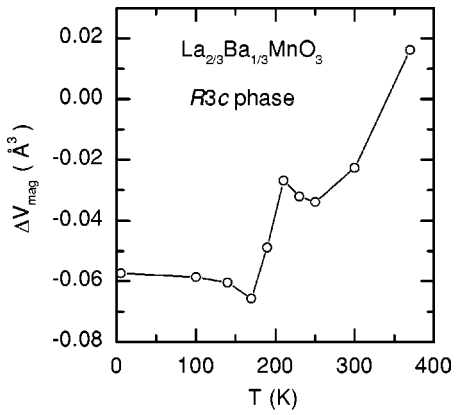

FIG. 12. The contribution ΔV_{mag} to the volume of the formula unit of $La_{2/3}Ba_{1/3}MnO_3$ caused by the magnetic phase transformations.

Here, $D(\theta_D/T)$ is the Debye function,[33] θ_D is the Debye temperature, V_0 is the volume at$T=0$, and A is determined by θ_D, compressibility and the Grüneisen constant of the substance. Supposing $\theta_D=400$ K (Ref. 34) in Eq. (5), we get $A=0.8867$ Å^3 and $V_0=59.362$ Å^3. Subtracting $V_{DG}(T)$ from the $V_{f.u.}(T)$ for the $R\bar{3}c$ phase, we get $V_{mag}(T)$ presented at Fig. 12.

As can be seen in Fig. 12, the $R\bar{3}c$ crystal volume contains two regions (140–210 K and 250 K), reflecting the magnetic phase transitions shown in Fig. 6. The steplike change of V_{mag} between 140 and 210 K reflects the first-order transition at $T_I=177.5\pm7.5$ K, whereas the singular point at 250 K reflects the second-order transition at $T_{II}=250$ K.

The main contribution to the change of V_{mag} at 140–210 K is coming from the crystal lattice parameter *a*, while for the corresponding contribution at 250 K the lattice parameter *c* is responsible.

Taking into account the possibility of a helical magnetic structure below 300 K, and at the same time, a similar to ordinary ferromagnetic behavior of χ between T_C and 300 K, we are obliged to suppose that $T_h=300$ K is a point of order-to-order phase transition of the second type.

The rather sharp steplike shapes of the curves in Fig. 2 mean that the studied compound undergoes the $R\bar{3}c\leftrightarrow Imma$ structural transformation in the vicinity of 200 K. At the first sight, this phase transition looks like a normal first-order phase transition. It has, however, some specific features: both phases are simultaneously present in different proportions on both sides far from 200 K and the relative content of the phases is only changing rather sharply in the 200 K region. This reminds of a martensitic phase transition.[35]

A peculiarity in the temperature range under discussion is seen rather well at the general picture of Bragg peaks caused by the nuclear and magnetic scattering in $La_{2/3}Ba_{1/3}MnO_3$ (Fig. 8). The integrated intensity of the first strong magnetic Bragg peak in Fig. 9 shows a change of slope at around 200 K. One can suppose that it is induced by the accelerated nuclear phase transformation $R\bar{3}c\leftrightarrow Imma$ at this temperature (Fig. 2).

The study carried out on the uniaxial pressure effect on the magnetic susceptibility $\chi=M/H$ has shown that the point $T_e=200$ K is a singular one of the temperature dependence of the $\Delta\chi/\chi$ value (Fig. 11), so the third derivative of the thermodynamic potential,

$$\frac{\partial^3\Phi}{\partial H\partial P\partial T}=\frac{\partial^2 M}{\partial P\partial T}, \tag{6}$$

has a break in this point. Such a singularity may be caused by a nonanalyticity of the electron states density $N(E)$ at the Fermi level. The crossing of singular point of the $N(E)$ function by the Fermi level, caused by a temperature transformation of the electronic structure and the Fermi distribution function, manifests itself as a so-called ''electronic transition.''[36] The ''electronic phase transitions'' can precede the conventional first- or second-order phase transitions, or take place simultaneously with the last ones.[36] The results obtained do not allow to assert unambiguously that there is a direct connection between the singularity of function (6) at the $T_e=200$ K point and the exchange of crystallographic phases around 200 K. They do not exclude such a possibility as well.

A possible cause of the complex temperature behavior of magnetic and lattice parameters of $La_{2/3}Ba_{1/3}MnO_3$, which differs radically from that of the related compound $La_{2/3}Ca_{1/3}MnO_3$[30] can be connected with a peculiarity of the electron structure of Ba^{2+} ion. The energies of $4f$ orbitals of this ion (which are vacant ones in a free Ba^{2+} ion) are sometimes very sensitive to the crystal-field potential values in oxide compounds.[37] The appearance of above-mentioned singularity of the $N(E)$ function at the Fermi level could be supposedly caused by a crossing of the Fermi level by the bottom of the ''falling'' vacant states band when the crystal potential of compound changes with temperature.

VI. CONCLUSION

(1) The uniform state of $La_{2/3}Ba_{1/3}MnO_3$ with the high-temperature crystallographic rhombohedral structure of the $R\bar{3}c$ space-group symmetry becomes unstable below the Curie point $T_C=314$ K and a small amount of the crystallographic phase of the *Imma* space-group orthorhombic structure appears in the system.

(2) The system undergoes two magnetic phase transitions in low magnetic fields below 300 K: of the second order at $T_{II}=250$ K and of the first order at $T_I=177.5$ K. The first-order transition shows 15 K clockwise temperature hysteresis.

(3) The compound passes via an exchange of the main structure phase $R\bar{3}c\leftrightarrow Imma$ in the vicinity of 200 K. The phenomenon looks as if the compound as a whole undergoes the first-order structural phase transition $R\bar{3}c\leftrightarrow Imma$ at $\approx$200 K, though both phases are present simultaneously in different proportions on both sides far from T_e. In some features this reminds of a martensitic phase transition.[35]

(4) The reduced change of magnetic susceptibility $\Delta\chi/\chi$ under uniaxial pressure displays a sharp minimum at $T_e=200$ K temperature.

(5) The temperature as well as field magnetic behavior of the compound in the temperature region between phase transitions T_C and T_{II}(314–250 K) is quite unusual for a collinear ferromagnet, its magnetic susceptibility is independent of temperature between 300 K and 250 K with good accuracy as well as of the applied low magnetic field, whereas it would have to change in the case of collinear magnets. This fact may be explained by the supposition that the magnetic structure of the system is not a collinear one and represents rather a long-period (of the order of several hundreds of angstroms) helix. The direct observation of such a complex structure meets a problem because of the large helix period and the small size of the metallic domains (10–50 nm) in the system.

(6) The revealed anomalies of the properties of $La_{2/3}Ba_{1/3}MnO_3$ (i.e., strong distinction from the properties of $La_{2/3}Ca_{1/3}MnO_3$ and $La_{2/3}Sr_{1/3}MnO_3$) can be caused by the peculiarity of the complex electronic structure of Ba^{2+} ion, the $4f$ shell of which (being vacant in the free atom) tends to a sharp lowering of the energy and decreasing of radius (so called ''collapse'') at certain values of the crystal-field potential in oxide compounds.[37,38]

APPENDIX A

An empirical formula for the susceptibility $\chi(H)$ representing the dashed lines at Fig. 7 looks as follows:

$$\chi(H)=\chi_0\frac{1+\xi\tanh\left(\frac{H}{H\kappa}\right)^p}{1+\psi\tanh\left(\frac{H}{H\eta}\right)^q}. \tag{A1}$$

It is obtained using low-field data ($H<0.1$ Oe) for the ac magnetic susceptibility of $La_{2/3}Ba_{1/3}MnO_3$.[39] Here, χ_0 is the initial susceptibility, H_κ, H_η, ξ, ψ, p, and q are considered as model parameters and are found by fitting Eq. (A1) to the experimental curve at Fig. 7. It was found that $\chi_0=1.4$, $\xi=23.7$, and $\psi=1.7$ at $T=290$ K. The corresponding values for $T=78$ K are 1.1, 16.9, and 1.2. The values $H_\kappa=0.0846$ Oe, $H_\eta=0.399$ Oe, $p=1.7$, and $q=0.65$ appeared to be equal for both temperatures.

The dependence in the form of Eq. (A1) describes general features of the low field $\chi(H)$ dependence of the $La_{2/3}Ba_{1/3}MnO_3$ compound. The main objective of Eq. (A1) is to obtain a magnitude of the susceptibility in the arbitrary point of the field interval considered, which is necessary for calculation of the effect of uniaxial pressure in a substance using Eq. (1) and the experimental data. At the same time, since the magnitudes of the parameters of Eq. (A1) may be of particular interest because they represent quantitative characteristics of the compound, it is a simple representation of the magnetic system of the compound. In this picture of the nonuniform system in weak fields $H<H_\eta$, a long-range magnetic order exists in the boundaries of separate magnetic domains, but in a certain interval of the fields higher than H_η, the system can be considered as a single-domain one with a high enough field induced magnetization. Physical sense of χ_0 is transparent (it was mentioned above), and the rest of the parameters can be phenomenologically qualitatively characterized on their function in the forming of the $\chi(H)$ curve: H_κ is the minimal local coercive force determining the initial running of susceptibility in a multi-domain case; H_η is the maximal local coercive force determining the moment of a transition to the single-domain state; p is an index of the curvature of the initial part of the $\chi(H)$ curve, it characterizes lability of the domain structure; q is an index of the field distribution of the local coercive forces, it characterizes an effective width of the field interval separating minimal and maximal magnitudes of the local coercive forces; ξ is an index of the maximal susceptibility of the multidomain structure; ψ (jointly with ξ) determines the susceptibility of the system in a single-domain state in weak magnetic fields (before a flipping of the supposed helical structure by the applied magnetic field).

APPENDIX B

On a microscopic model level, the appearance of helical magnetic structures is usually being explained by the competition between the positive exchange of the nearest atomic neighbors and the negative exchange between the next to the nearest neighbors (this is provided, for example, by the Ruderman-Kittel-Kasuya-Yosida indirect exchange model, which was among others also proposed for manganites[40]). So magnetic susceptibility may be written as follows:[24,25]

$$\chi_h=\frac{9\mu_B^2}{16k_BV_{f.u.}|J_2|\left(1-\frac{J_1}{4|J_2|}\right)^2\left[1+\frac{J_1}{2|J_2|}\left(1+\frac{J_1}{4|J_2|}\right)\right]}. \tag{B1}$$

Here μ_B is Bohr magneton, k_B is Boltzmann constant, $V_{f.u.}$ is the volume of a formula unit of the substance, $J_1>0$ and $J_2<0$ are the exchange integrals for the first and the second coordination spheres, respectively. The helix angle α is determined by the equation

$$\cos\alpha=-\frac{J_1}{4J_2}. \tag{B2}$$

If one evaluates the exchange integral J_1 using the molecular-field model as

$$J_1=\frac{3k_BT_C}{2zS(S+1)}, \tag{B3}$$

where the number of the nearest neighbors of the Mn ion is $z=6$, the spin of the Mn^{3+} ion is $S=3/2$, and $T_C=314$ K, then $J_1\approx24.5$ K. Using Eqs. (B1) and (B2) and taking into account values $\chi=13.67$ (from the experiment) and $J_1=24.5$ K [from Eq. (B3)], we get $J_2\approx-6.16$ K, $\alpha\approx5.8°$, and the period of the helical structure of about 238 Å, i.e., of about $18c$ for the $R\bar{3}c$ structure or $30b$ for the $Imma$ one.

APPENDIX C

Intensity I of the Bragg magnetic diffraction peak is connected with magnetic structure by the following way:[41,42]

$$I \propto \sum_{\alpha,\beta} \left(\delta_{\alpha,\beta} - \frac{\kappa_\alpha \kappa_\beta}{\kappa^2} \right) \langle S_\kappa^\alpha \rangle \langle S_{-\kappa}^\beta \rangle. \tag{C1}$$

Here $\alpha,\beta = x,y,z$ are the coordinate axes indices, κ is a transferred momentum, $\delta_{\alpha,\beta}$ is the Kronecker delta, $S^\alpha(\kappa)$ is a Fourier transform of electron spins, and the angular brackets denote statistical average. Nonzero values of I correspond to $\kappa = \mathbf{G}$, where $\mathbf{G}$ is a vector of the reciprocal magnetic lattice.

In a simple ferromagnetic structure, we have $S_\kappa^\alpha = S_\kappa^Z \delta_{\alpha,Z}$ (Z is an easy magnetization axis or a direction of an infinitesimal external magnetic field in case of a zero magnetic crystalline anisotropy), $\mathbf{G} = \mathbf{g}$ ($\mathbf{g}$ is a vector of the reciprocal crystal lattice), so, the Eq. (C1) is simplified to

$$I_{FM} \propto \langle S^Z \rangle^2 \sum_{\mathbf{g}} |f(\mathbf{g})|^2 \left[1 - \left(\frac{\kappa^Z}{\kappa} \right)^2 \right] \delta_{\kappa,\mathbf{g}}, \tag{C2}$$

where $f(\mathbf{g})$ is a magnetic form factor. For a long-period magnetic superstructure (period L_h of which is much more than a lattice constant c), representing a long-wave modulation of the "initial" ferromagnetic structure, we have $\mathbf{G} = \mathbf{g} + \mathbf{q}$, where $\mathbf{q}$ is of order of the propagation vector of the superstructure and thus it is rather small: $\mathbf{q} \sim 2\pi/L_h \ll \mathbf{G} \sim 2\pi/c$. Taking, however, into account that magnetically ordered regions in manganites are very small (they are clusters of sizes $L \sim L_h$ or even $L < L_h$, see Introduction and Appendix B), we cannot expect an observation of a resolved diffraction peak corresponding to a magnetic structure with the propagation vector $\mathbf{q} \sim 2\pi/L_h$ because of too high uncertainty $\Delta\mathbf{G}$ of the vector $\mathbf{G}$ of the reciprocal magnetic lattice: $\Delta\mathbf{G} = 2\pi/L \sim 2\pi/L_h \sim \mathbf{q}$. Instead, in such conditions we can see only a unified magnetic peak indistinguishable from a "coarse" magnetic structure,[23] i.e., from the ferromagnetic one (C2). The temperature dependence of the square root of I in Eq. (C1) will reflect the thermal average of the projection of the site spin onto local quantization axis ζ: $I^{1/2} \propto \langle S^\zeta \rangle$. For a true ferromagnetic structure $I_{FM}^{1/2} \propto \langle S^Z \rangle$, as it follows from Eq. (C2). For small enough magnetic clusters, there is no visible difference between the diffraction spectrum of a long-period superstructure and a simple ferromagnetic. So we can consider an effective ferromagnetic structure instead of a supposed superstructure. Thus, the square root of the intensity in Eq. (C1) can be considered as a value reflecting a Z projection of an atomic spin in an "equivalent" ferromagnetic structure, i.e., as an "effective" (responsible for the total intensity of a possible unresolved peak) atomic magnetic moment. It may differ from a real thermal average of the atomic spin Z projection if the magnetic structure is not a simple ferromagnetic one.

*Corresponding author. Elena L. Fertman, Institute for Low Temperature Physics and Engrg., 47 Lenin Avenue, Kharkov 61103, Ukraine. Email address: Fertman@ilt.kharkov.ua; FAX: 38-0572-335593.

[1] E. Dagotto, T. Hotta, and A. Moreo, Phys. Rep. **344**, 1 (2001).
[2] J.M.D. Coey, M. Viret, and S. von Molnar, Adv. Phys. **48**, 167 (1999).
[3] V.M. Loktev and Yu.G. Pogorelov, Low Temp. Phys. **26**, 171 (2000).
[4] M.B. Salamon and M. Jaime, Rev. Mod. Phys. **73**, 583 (2001).
[5] J.M. De Teresa, M.R. Ibarra, P.A. Algarabel, C. Ritter, C. Marquina, J. Blasco, J. Garcia, A. del Moral, and Z. Arnold, Nature (London) **386**, 256 (1997).
[6] P.G. Radaelli, G. Iannone, M. Marezio, H.Y. Hwang, S-W. Cheong, J.D. Jorgensen, and D.N. Argyriou, Phys. Rev. B **56**, 8265 (1997).
[7] E.O. Wollan and W.C. Koehler, Phys. Rev. **100**, 545 (1955).
[8] J.B. Goodenough, Phys. Rev. **100**, 564 (1955).
[9] C. Zener, Phys. Rev. **82**, 403 (1951).
[10] P.W. Anderson and H. Hasegawa, Phys. Rev. **100**, 675 (1955).
[11] A.J. Millis, B.I. Shraiman, and R. Mueller, Phys. Rev. Lett. **77**, 175 (1996).
[12] F. Cordero, C. Castellano, R. Cantelli, and M. Ferretti, Phys. Rev. B **65**, 012403 (2001).
[13] J.M. De Teresa, C. Ritter, M.R. Ibarra, P.A. Algarabel, J.L. Garcia-Munoz, J. Blasco, J. Garcia, and C. Marquina, Phys. Rev. B **56**, 3317 (1997).
[14] J.W. Lynn, R.W. Erwin, J.A. Borchers, Q. Huang, A. Santoro, J.-L. Peng, and Z.Y. Li, Phys. Rev. Lett. **76**, 4046 (1996).
[15] M. Fath, S. Freisen, A.A. Menovsky, Y. Tomioka, J. Aarts, and J.A. Mydosh, Science **285**, 1540 (1999).
[16] G. Papavassiliou, M. Fardis, M. Belesi, T.G. Maris, G. Kallias, M. Pissas, D. Niarchos, C. Dimitropoulos, and J. Dolinsek, Phys. Rev. Lett. **84**, 761 (2000).
[17] S.E. Lofland, S.M. Bhagat, H.L. Ju, G.C. Xiong, T. Venkatesan, and R.L. Greene, Phys. Rev. B **52**, 15 058 (1995).
[18] S.J.L. Billinge, Th. Proffen, V. Petkov, J.L. Sarrao, and S. Kycia, Phys. Rev. B **62**, 1203 (2000).
[19] N. Moutis, I. Panagiotopoulos, M. Pissas, and D. Niarchos, Phys. Rev. B **59**, 1129 (1999).
[20] W. Archibald, J.-S. Zhou, and J.B. Goodenough, Phys. Rev. B **53**, 14 445 (1996).
[21] S.N. Barilo, G.L. Bychkov, L.A. Kurnevich, S.V. Shiryaev, L.A. Kurochkin, J.W. Lynn, and L. Vasiliu-Doloc, J. Cryst. Growth **211**, 480 (2000).
[22] I.O. Troyanchuk, D.D. Khalyavin, S.V. Trukhanov, and H. Szymczak, J. Phys.: Condens. Matter **11**, 8707 (1999).
[23] I.E. Dzyaloshinsky, Zh. Eksp. Teor. Fiz. **46**, 1420 (1964); **47**, 336 (1964); **47**, 992 (1964).
[24] A. Herpin and P. Meriel, Compt. Rend. **250**, 1450 (1960); J. Phys. Radium **22**, 337 (1961).
[25] K.P. Belov, M.A. Belyanchikova, R.Z. Levitin, and S.A. Nikitin, *Rare-Earth Ferromagnets and Antiferromagnets* (Nauka, Moscow, 1965) (in Russian).
[26] A.B. Beznosov, E.L. Fertman, V.A. Desnenko, and D.D. Khalyavin, J. Magn. Magn. Mater. **241**, 69 (2002).
[27] V.A. Desnenko, A.S. Panfilov, and A.I. Smirnov, Low Temp. Phys. **21**, 424 (1995).

[28] J. Rodriguez-Carvajal, Physica B **192**, 55 (1993).
[29] H.L. Ju, J. Gopalakrishnan, J.L. Peng, Q. Li, G.C. Xiong, T. Venkatesan, and R.L. Greene, Phys. Rev. B **51**, 6143 (1995).
[30] A.B. Beznosov, B.I. Belevtsev, E.L. Fertman, V.A. Desnenko, D.G. Naugle, K.D.D. Rathnayaka, and A. Parasiris, Fiz. Nizk. Temp. **28**, 774 (2002) [Low Temp. Phys. **28**, 556 (2002)].
[31] A.B. Beznosov, E.L. Fertman, and P.P. Pal'-Val', J. Magn. Magn. Mater. **192**, 111 (1999).
[32] C.W. Searle and S.T. Wang, Can. J. Phys. **48**, 2073 (1970).
[33] L.D. Landau and E.M. Lifshits, *Statistical Physics* (Nauka, Moscow, 1976) (in Russian).
[34] J.J. Hamilton, E.L. Keatley, H.L. Ju, A.K. Raychaudhuri, V.N. Smolyaninova, and R.L. Greene, Phys. Rev. B **54**, 14 926 (1996).
[35] J.W. Christian, *The Theory of Transformations in Metals and Alloys* (Pergamon Press, Oxford, 1965).
[36] I.M. Lifshits, Zh. Eksp. Teor. Fiz. **38**, 1569 (1960) [Sov. Phys. JETP **11**, 1130 (1960)].
[37] N.G. Stoffel, J.M. Tarascon, Y. Chang, M. Onellion, D.W. Niles, and G. Margaritondo, Phys. Rev. B **36**, 3986 (1987).
[38] V.V. Nemoshkalenko, V.Kh. Kas'yanenko, B.G. Nikitin, L.I. Nikolaev, Yu.G. Pogorelov, G.A. Klimenko, and P.V. Gel', Sverkhprovodimost' (KIAE) **2**, 41 (1989) [Superconductivity **2**, 47 (1989)].
[39] A.B. Beznosov, V.V. Eremenko, E.L. Fertman, V.A. Desnenko, and D.D. Khalyavin, Fiz. Nizk. Temp. **28**, 1065 (2002) [Low Temp. Phys. **28**, 762 (2002)].
[40] E.L. Nagaev, Usp. Fiz. Nauk **166**, 833 (1996) [Phys. Usp. **39**, 781 (1996)].
[41] G.E. Bacon, *Neutron Diffraction*, 3rd ed. (Clarendon Press, Oxford, 1975).
[42] R.M. White, *Quantum Theory of Magnetism* (Springer-Verlag, Berlin, 1983).